



Calcification Detection in Coronary Arteries Using Image Processing

Pankaj Goyal*

Department of Electrical Engineering,
DCRUST, Murthal,
Sonapat, India

Kuldeep Goyal

Scientist, DIPR, Defence R & D
Organization (DRDO),
Delhi, India

Vipin Gupta

Senior Scientist, Philips
Research, Manyata Tech
Bangalore, India

Abstract— The paper discusses the calcification detection in the coronary arteries of the heart using image processing. The source data is filtered using two dimensional DICOM (Digital imaging and Communications in Medicine) images taken from the 64-slice Computed Tomography Scan data of the heart using a vessel enhancement diffusion filter to highlight only the regions containing coronary arteries. The segmentation of coronary arteries of the heart has been implemented on two dimensional Computed Tomography (CT) isolated data. The 64- slice CT scan technology provides a non-invasive method to directly visualize the coronary arteries. The angiography using 64-slice CT scan machine provides better visualization of the coronary arteries using a small dose of contrast, which was difficult to achieve with earlier imaging techniques. The system has been developed using different image processing functions in MATLAB environment. The calcification regions in different arteries using this system are labelled by blue colour.

Keywords— Computed Tomography Angiography; Digital Subtraction Angiography; Coronary Artery Diseases; Segmentation; Morphological operations; Hessian.

I. INTRODUCTION

Coronary artery disease (CAD) is the leading cause of death in western countries. CAD is the single most important cause of death in India, Australia, New Zealand & other countries. Every year, billions of dollars have been spent in the treatment of coronary artery disease also. Given the invasiveness of coronary angiography and potential danger of having a small risk of serious complications (arrhythmia, stroke, coronary-artery dissection and death), a non-invasive technique for imaging of the coronary artery disease is highly desirable. Imaging of the heart and coronary artery branches has always been challenging due to the heart's continuous movement. Over the past decade, great steps have been taken in the field of cardiac imaging as non-invasive coronary imaging modalities have undergone rapid developments [1-4].

Calcified lesions in the coronary arteries are the main indicators of CAD. These calcified lesions are found to be within the five main coronary arteries, the Left Main (LM), Left Anterior Descending (LAD), Left Circumflex (LCX), Posterior Descending (PDA) and the Right Coronary artery (RCA). The most reliable way & invasive procedure to diagnose coronary artery disease, the catheterization is costly, time consuming, and has risks. Image processing modes based on radiographic views may not completely provide diagnostic information at an early stage to control a disease, make a therapeutic decision, or perform surgery. This lack of timely information requires some further processing of images to detect tumors, lesions and blockage. Coronary computed tomography angiography (CTA) is a heart imaging test that helps determine if deposits of fat or calcium (plaque) have narrowed a patient's coronary arteries. Coronary CTA is a special type of x-ray examination. Patients undergoing a coronary CTA scan receive an iodine-containing contrast material (dye) as an intravenous (IV) injection to ensure the best possible images. CT scans of internal organs, bones, soft tissue and blood vessels provide greater clarity and reveal more details than regular X-Ray examinations [5]. The coronary CT angiography studies are very promising and exciting. Since 1993 coronary MR angiography has been performed with temporal resolution of 40-100 ms [5]. Because the 64-slice CT scanner offers faster gantry rotation, as low as 330 milliseconds, and smaller detector arrays, it allows higher temporal and spatial resolution. The 64-slice CT scanner can visualize the entire heart in less than 10 seconds, revealing blockages in blood vessels and other heart problems that are sometimes not easily detectable with other tests [6-9, 10].

Image segmentation facilitates delineation of anatomical structures and other regions of interest. Segmentation is one of the most difficult tasks in image processing and determines the outcome of analysis and evaluation of pathological regions

II. LITERATURE SURVEY

Segmentation of the vascular tree will facilitate volumetric display and will enable quantitative measurements of vascular morphology. There are several techniques for the enhancement of vessels. Some of these techniques worked at a fixed scale and use combinations of finite difference operators applied in a set of orientations [24-26]. Orkisz presents a method that applies a median filter in the direction of the vessel [19]. All these methods have shown problems to detect vessels over a large size range since they perform a fixed scale analysis. To handle voxel anisotropy, these methods usually need to resample the dataset or to resource to 2.5-D processing (cf. [23]). Multi-scale techniques to the enhancement of vessels include "cores" [14] and assessment of local directions through eigen-value analysis of the Hessian matrix [21, 13]. The multi-scale approach is inspired by the work of Sato *et al.* [13] and Lorenz *et al.* [14] who

use the Eigen values of the Hessian to determine locally the likelihood that a vessel is present. We consider all Eigen values and giving the vesselness measures an intuitive, geometric interpretation.

Level-set-based active contour methods to vessels extraction were discussed in Reference 29, whose gradient information was used. The evolution can be implemented by Fast Marching algorithm, because all the speed in the image is defined as the positive or negative speed fields. Most of the methods are sensitive to the initial condition. Region-based methods are more suitable for vessel segmentation because the whole region information, not only boundary gradient information, is considered. Early region-based method is Markov random fields-based approach. Recently, many region-based active contour models were presented. Yezzi presented a global approach for image segmentation [20], but it has too extensive computational cost. The geodesic active region model, who integrates boundary-based with region-based active contour approaches presented by Nikos [28], is more effective than region-based segmentation methods, because the prior knowledge about ROI is introduced. We have used Vessel Enhancement Diffusion filtering developed by A. Frangi to enhance/Segment the vessels/Coronary arteries.

III. METHODS

The two dimensional CT scan image of heart from the DICOM data obtained from the 64- slice CT scan machine provides a image which is an image from the sequence of images taken from different projections by rotating the gantry. This image provides the view of some of the coronary arteries of the heart at that projection at which we have chosen an image to process further for calcification detection. For the detection of calcification regions in the arteries, we must segment the coronary arteries in such a proper way that can be used for further processing to measure the diameter of arteries thoroughly. The image is showing the coronary arteries along with the other parts of the heart. Since, we are interested in the coronary arteries only, so other regions of the image are just like a noise for us and so must be filtered so that we can segment the coronary arteries and apply processing to detect the calcification. The used steps in the method are described below.

A. Vessel Enhancement Diffusion Filter:

A vesselness measure is obtained on the basis of all Eigen values of the Hessian. In our approach we conceive vessel enhancement as a filtering process that searches for geometrical structures which can be regarded as tubular. Since vessels appear in different sizes it is important to introduce a measurement scale which varies within a certain range [16].

An approach to analyse the local behaviour of an image, L , is by considering its Taylor series expansion in the neighbourhood of a point X_0 ,

$$L(X_0 + \delta X_0, s) \approx L(X_0, s) + \delta X_0^T \Delta_0, s + \delta X_0^T H_{0, s} \delta X_0 \quad (1.1)$$

This Taylor's series expansion of an image L approximates the structure of the image up to second order. Δ_0, s and $H_{0, s}$ are the gradient vector and Hessian matrix of the image computed in X_0 at scale s . To calculate these differential operators, we use concepts of linear scale space theory [16]. Differentiation is defined as a convolution with derivatives of Gaussians:

$$\frac{\partial L(x, s)}{\partial x} = s^\gamma L(x) \cdot \frac{\partial G(x, s)}{\partial x} \quad (1.2)$$

where the D-dimensional Gaussian is defined as:

$$G(x, s) = \frac{1}{\sqrt{2\pi}^D} e^{-\frac{\|x\|^2}{2s^2}} \quad (1.3)$$

The parameter γ was introduced to define a family of normalized derivatives for the comparison of the response of differential operators at multiple scales. When no scale is preferred γ should be set to unity [12]. The second derivative of a Gaussian kernel at scale s generates a probe kernel that measures the contrast between the regions inside and outside the range $(-s, s)$ in the direction of the derivative.

The third term in Equation (1.1) gives the second order directional derivative,

$$H_{0, s} \delta X_0^T \delta X_0 = \frac{\partial}{\partial \delta X_0} \frac{\partial}{\partial \delta X_0} L(X_0, s) \quad (1.4)$$

The objective of eigen-value analysis of the Hessian is to extract the principal directions in which the local second order structure of the image can be decomposed. Since this directly gives the direction along the vessel.

$$H_{0, s} \hat{u}_{s, k}^T \hat{u}_{s, k} = \lambda_{s, k} \hat{u}_{s, k} \quad (1.5)$$

Let $\lambda_{s, k}$ denote the Eigen value corresponding to the k -th normalized eigenvector $\hat{u}_{s, k}$ of the Hessian $H_{0, s}$ all computed at scale s . From the definition of Eigen values and it follows that

$$H_{0, s} \hat{u}_{s, k} = \lambda_{s, k} N_{X_0} \quad (1.6)$$

By analysing Equations (1.4)-(1.6) a nice geometric interpretation arises. The Eigen value decomposition extracts three ortho-normal directions which are invariant up to a scaling factor when mapped by the Hessian matrix.

λ_k will be the Eigen value with the k -th smallest magnitude ($|\lambda_1| < |\lambda_2| < |\lambda_3|$). In particular, a pixel belonging to a vessel region will be signalled by λ_1 being small (ideally zero), and λ_2 and λ_3 of a large magnitude and equal sign and the sign is an indicator of brightness or darkness. The respective eigenvectors point out singular directions: \hat{u}_1 indicates the direction along the vessel and \hat{u}_2 and \hat{u}_3 form a base for the orthogonal plane. In CTA, vessels emerge as bright tubular structures in a darker environment. This prior information of the imaging modality can be used as a check to discard structures present in the dataset with a polarity different than the one found. Accordingly, we shall look for structures whose λ_2 and λ_3 are both simultaneously negative. To summarize, for an ideal tubular structure in a 3D image:

$$|\lambda_1| \approx 0 \quad (1.7)$$

$$\begin{aligned} |\lambda_1| &\ll |\lambda_2| \\ \lambda_2 &\approx \lambda_3 \end{aligned} \quad (1.8) \quad (1.9)$$

and the sign of λ_2 and λ_3 indicate its polarity.

All three Eigen values will yield expressions that differ from the similarity measures proposed by Sato *et al.* [13] and Lorenz *et al.* [14] that only make use of two Eigen values in their respective 3D line filters.

We used a measure that takes into account two geometric ratios based on the second order ellipsoid. The first ratio accounts for the deviation from a blob-like structure but cannot distinguish between a line- and a plate-like pattern.

$$R_B = \frac{\text{Volume} / 4\pi/3}{(\text{Largest Cross Section Area} / \pi)^{3/2}} = \frac{|\lambda_1|}{\sqrt{|\lambda_2\lambda_3|}} \quad (1.10)$$

This ratio attains its maximum for a blob-like structure and is zero whenever $\lambda_1 \approx 0$, or λ_1 and λ_2 tend to vanish.

The second ratio accounts for the aspect ratio of the two largest second order derivatives. This ratio is essential for distinguishing between plate-like and line-like structures since only in the latter case it will be zero,

$$R_A = \frac{\text{Largest Cross Section Area} / \pi}{(\text{Largest Axis Semi Length})^2} = \frac{|\lambda_2|}{|\lambda_3|} \quad (1.11)$$

These two geometric ratios remain constant under intensity rescaling. This ensures that our measures only capture the geometric information of the image. We define the following measure of "second order structureness",

$$S = \|H\|_F = \sqrt{\sum_{j \leq D} \lambda_j^2} \quad (1.12)$$

This measure will be low in the background where no structure is present and the Eigen values are small for the lack of contrast. In regions with high contrast compared to the background, the norm will become larger since at least one of the Eigen values will be large. We therefore define a following vesselness function,

$$v_0(s) = \begin{cases} 0 & \text{if } \lambda_2 > 0 \text{ or } \lambda_3 > 0 \\ (1 - \exp(-\frac{R_A^2}{2\alpha^2})) (\exp(-\frac{R_B^2}{2\beta^2})) (1 - \exp(-\frac{S^2}{2c^2})) & \text{otherwise} \end{cases} \quad (1.13)$$

where α , β and c are thresholds which control the sensitivity of the line filter to the measures R_A , R_B and S . We combine the different criteria using their product to ensure that the response of the filter is maximal only if all three criteria are fulfilled. The vesselness measure of Equation (1.13) is analysed at different scales s . The response of the line filter will be a maximum at a scale that approximately matches the size of the vessel to detect. We have final estimate of vesselness measure provided by the filter response at different scales:

$$v_0(\gamma) = \max_{s_{\min} \leq s \leq s_{\max}} v_0(s, \gamma) \quad (1.14)$$

where s_{\min} and s_{\max} are the maximum and minimum scales at which vessels are expected to be found. They can be so chosen as to cover the range of vessel widths. For 2D images we will have the following vesselness measure,

$$v_0(s) = \begin{cases} 0 & \text{if } \lambda_2 > 0, \\ (\exp(-\frac{R_B^2}{2\beta^2})) (1 - \exp(-\frac{S^2}{2c^2})) & \text{otherwise} \end{cases} \quad (1.15)$$

The gray scale image obtained after conversion from the original input image and the images obtained after the application of Vessel Enhancement Diffusion Filter are shown as follows:



Fig.1 (a) Greyscale Image obtained from Original Input Image Fig1. (b) Image obtained after Vessel Enhancement Diffusion Filter

B. Morphological Operations

Morphological operations are broad set of image processing operations that process images based on shapes. Morphological operations apply a structuring element to modify the value of each pixel in the output image is based on a comparison of the corresponding pixel in the input image with its neighbours [12].

- 1) *Morphological Dilation and Erosion:* The most basic morphological operations are dilation and erosion. Dilation adds pixels to the boundaries of objects in an image, while erosion removes pixels on object boundaries. The number of pixels added or removed from the objects in an image depends on the size and shape of the structuring element used to process the image. In the morphological dilation and erosion operations, the state of

any given pixel in the output image is determined by applying a rule to the corresponding pixel and its neighbours in the input image [12]. Dilation and erosion are often used in combination to implement image processing operations.

- 2) *Morphological Opening and Closing*: The definition of a morphological opening of an image is erosion followed by dilation, using the same structuring element for both operations. The related operation, morphological closing of an image, is the reverse: it consists of dilation followed by erosion with the same structuring element. You can use morphological opening to remove small objects from an image while preserving the shape and size of larger objects in the image [11].

TABLE: 1.2 DILATION- AND EROSION-BASED FUNCTIONS

<i>Function</i>	Morphological Definition
<i>Imclose</i>	Dilates an image and then erodes the dilated image using the same structuring element for both operations.
<i>Imopen</i>	Erodes an image and then dilates the eroded image using the same structuring element for both operations.

C. Distance Transform

The distance transform provides a metric or measure of the separation of points in the image. The *bwdist* function calculates the distance between each pixel that is set to off (0) and the nearest nonzero pixel for binary images [11].

After the application of filtering & different morphological operation, we got the image with segmented coronary arteries which are shown in figure 2(a). The image with the segmented arteries was overlaid on the original RGB image and is shown in figure 2(b).

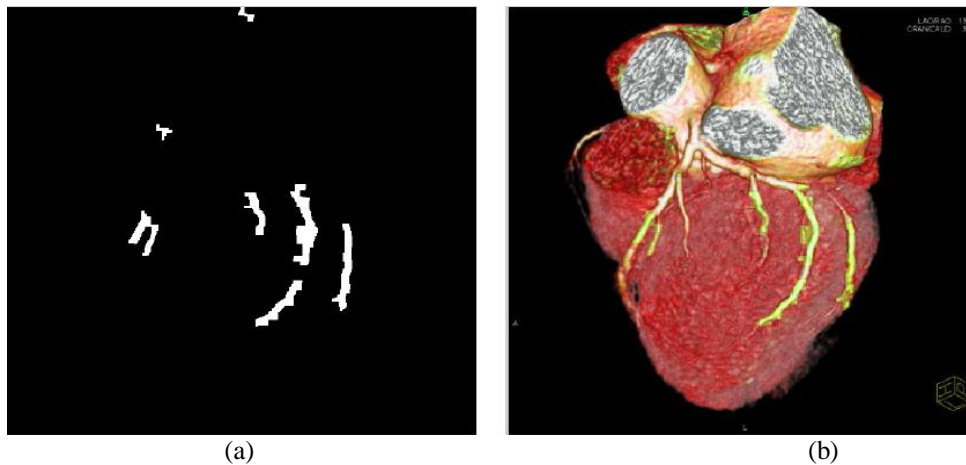


Fig.2 (a) Image of Segmented Coronary Arteries; (b) Image obtained after overlaying the image with segmented Coronary Arteries on the original Input image

The images obtained at different stages of the method described are as follows:

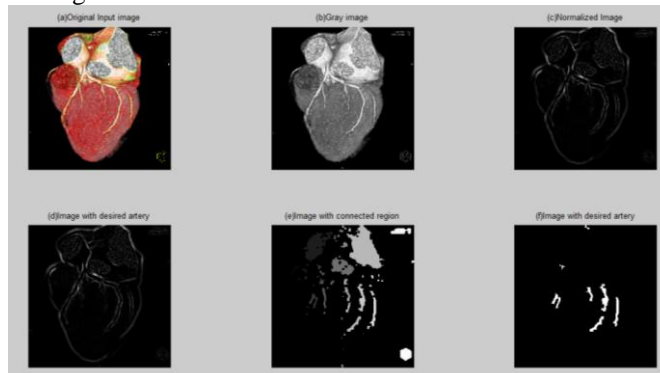


Fig.3 Images at Different stages (a) Original RGB DICOM image; (b) Gray scale image obtained from RGB image; (c) Image after normalization; (d) Image after Filtering;(e) Image with Connected Regions; (f) Image with segmented coronary arteries.

IV. EXPERIMENTS AND RESULTS

To evaluate the described method, we used the 5 data sets of DICOM images obtained from the normal & abnormal person; the described method gave satisfactory results by detecting the calcification in the arteries of abnormal patient data i.e. the patient with calcification in the arteries. The output of the method described, shows the Vessel/Coronary Artery diameter plot along with the region of calcification in the figures 4 and 5 below.

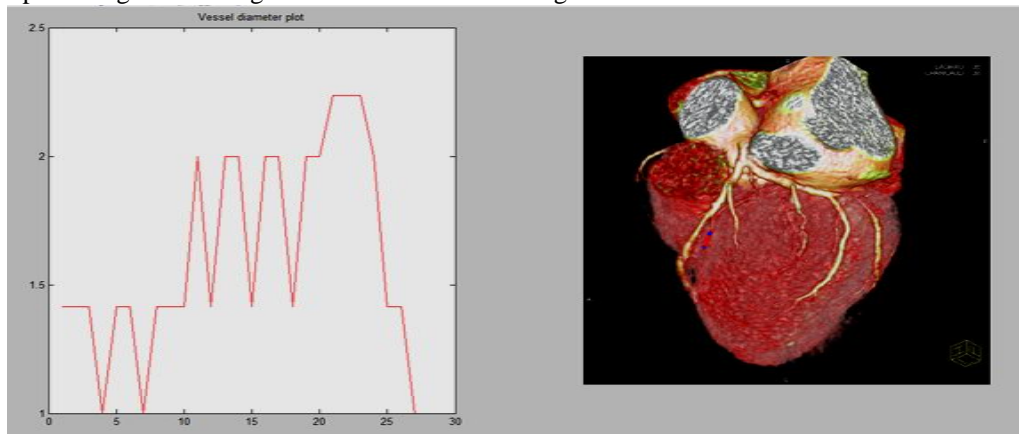


Fig.4 Artery/Vessel diameter plot with Calcification region shown by blue colour & non-calcified region shown by Red colour in First patient's data.

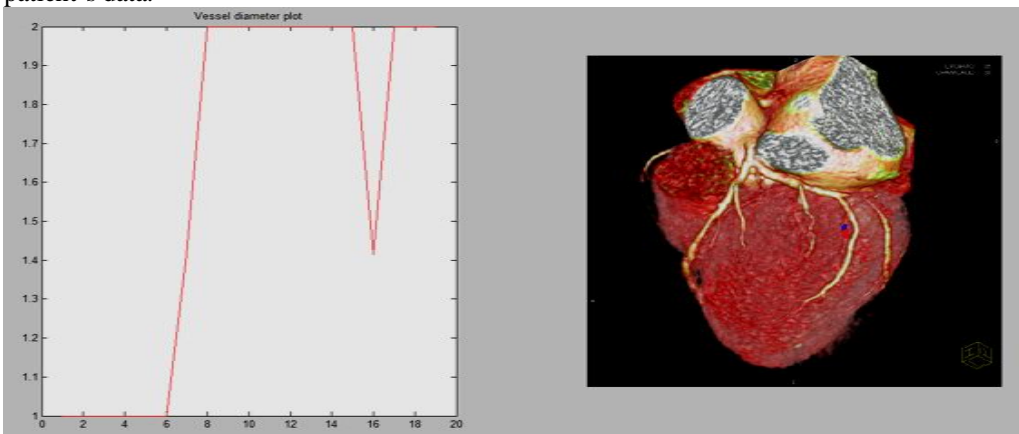


Fig.5 Coronary Artery/Vessel diameter plot with Calcification region shown by blue colour & non-calcified region shown by Red colour in first patient's data.

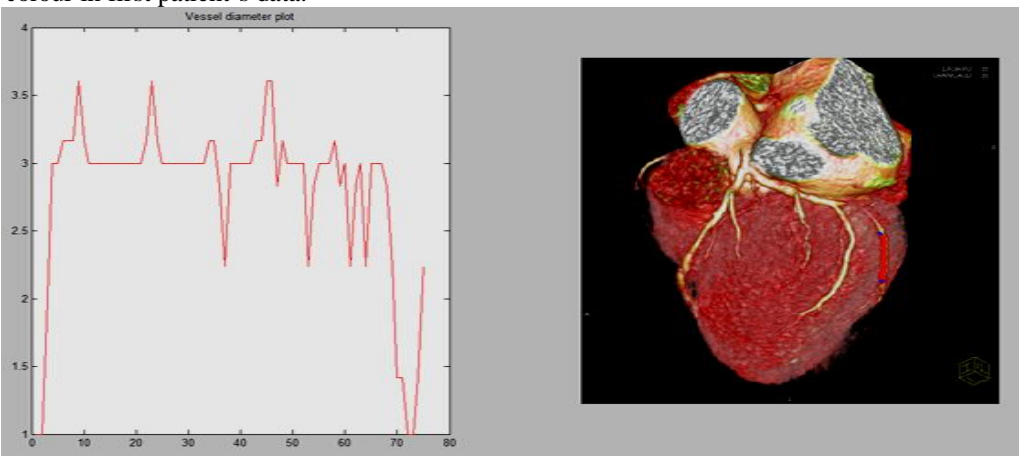


Fig. 6 Coronary Artery/Vessel diameter plotted with Calcification region shown by blue colour & non-calcified region shown by Red colour in data of another patient.

V. CONCLUSIONS

We have described a method for the detection of calcification in the coronary arteries/vessels in the heart of an abnormal person which has calcifications in the arteries/vessels. The method was applied on the data obtained from the 64 slice computed tomography scan machine. The method was implemented on the Intel(R) core (TM) i3 at 2.20GHz using MATLAB version 7.8.0.347 and tested with many DICOM files obtained from different orientation of CT scan machine to provide different coronary arteries of heart the method is showing the calcification regions by labelling the region with a colour different from that of original image. The measurement of percentage of calcification can be done in the future scope of the research. From the measurement of percentage of calcification, severity of the blockage can be estimated and required appropriate treatment can be given to patient.

References

- [1]. K Nieman, M. Oudkerk, B.J. Rensing, P. Van Ooijen, A. Munne, R.J. Van Geuns, P.J De Feyter, "Coronary angiography with multi-slice computed tomography". *Lancet*. Vol. 357 No. 9256, pp. 599-603, 2001.
- [2]. P.G. O'Malley, A.J. Taylor, J.L. Jackson, T.M. Doherty; R.C. Detrano, "Prognostic value of coronary electron-beam computed tomography for coronary artery disease events in asymptomatic populations", *American Journal of Cardiology*, Vol. 87, pp. 1335-1339, 2001.
- [3]. P.G. Dianas, A. Roussakis, P.A. Ioannidis John, "Diagnostic performance of coronary magnetic resonance angiography as compared against conventional X-ray angiography: A Meta-Analysis", *J Am Coll Cardiol*. Vol. 44, No. 9, pp. 1867-1876, 2004.
- [4]. J.P. Finn, K. Nael, V. Deshpande, O. Ratib, G Laub, "Cardiac MR imaging: State of the Technology". *Radiolog*, Vol. 241, No. 2, pp. 338-354, 2006.
- [5]. (2012) The RADIOLOGY website. [Online]. Available <http://www.radiologyinfo.org/en/info.cfm?pg=angiocoroct>.
- [6]. A.J. Duerinckx, "Coronary Magnetic Resonance Angiography", New York: Springer-Verlag, pp. 342. 2002.
- [7]. P.De Feyter, G. P. Krestin, "Computed Tomography of the Coronary arteries", United Kingdom: Taylor & Francis, pp. 208. 2005.
- [8]. M. Oudkerk, "Coronary Radiology", Springer-Verlag, pp. 293. 2004.
- [9]. Schoenhagen P., Steven E. Nissen, "Atlas and Manual of Coronary Intravascular Ultrasound Imaging", Taylor & Francis Group, pp. 147. 2004.
- [10]. O.M Vanovermeire, A.J. Duerinckx, "A Practical Approach to 64-slice Coronary CT Angiography", *JBR-BTR*, Vol. 89, pp. 1-7, 2006.
- [11]. MATLAB Software/ Help Documentation.
- [12]. T. Lindeberg, "Edge detection and ridge detection with automatic scale selection", Proceedings of Conference on Computer Vision and Pattern Recognition, San Francisco, CA, pp. 465-470. 1996.
- [13]. Y. Sato, S. Nakajima, H. Atsumi, T. Koller, G Gerig, S. Yoshida, R. Kikinis, "3D multi-scale line filter for segmentation and visualization of curvilinear structures in medical images", IEEE First joint conference on Computer Vision, Virtual Reality and Robotics in Medicine and Medical Robotics and Computer-Assisted Surgery, Vol. 1205, pp. 213-222, 1997.
- [14]. C. Lorenz, I.C. Carlsen, T.M. Buzug, C. Fassnacht, J. Wesse, "Multi-scale line segmentation with automatic estimation of width, contrast and tangential direction in 2D and 3D medical images", Proceedings of First Joint Conference, Computer Vision, Virtual Reality and Robotics in Medicine and Medical Robotics and Computer-Assisted Surgery, Vol 1205, pp. 233-242, 1997.
- [15]. A. F. Frangi, W.J. Niessen, K.L. Vincken, M.A. Viergever, "Multiscale vessel enhancement Filtering", MICCAI'98 Medical Image Computing and Computer-Assisted Intervention, Lecture Notes in Computer Science, Springer Verlag, Vol. 1496, pp. 130-137, 1998.
- [16]. H. Chen, "An algorithm for MR angiography image enhancement", *Magnetic Resonance in Medicine*, Vol. 33, No. 4, pp. 534- 540, 1995.
- [17]. Y. E. Du, "Vessel enhancement filtering in three-dimensional MR Angiography", *Magnetic Resonance Imaging*. Vol. 5, No.3, pp. 353-359, 1995.
- [18]. Y. P. Du, "Vessel enhancement filtering in three dimensional MR angiograms using long range signal correlation", *Magnetic Resonance Imaging*, Vol. 7, No. 2, pp. 447-450, 1997.
- [19]. M.M. Orkisz, C. Bresson, I.E. Magnin, O.Champin, P.C. Douek,, "Improved vessel visualization in MR angiography by nonlinear anisotropic filtering", *Magnetic Resonance in Medicine*, Vol. 37, No. 6, pp. 914-919, 1997.
- [20]. A. Jr. Yezzi; A. Tsai; A. Willsky, "A fully global approach to image segmentation via coupled curve evolution equations", *Journal of Visual Communication and Image Representation*. Vol. 13, pp. 195-216, 2002.
- [21]. T.M. Koller, "From Data to Information: Segmentation, Description and Analysis of the Cerebral Vasculature", Dissertation ETH No. 11367, Swiss Federal Institute of Technology ETHZ. 1995.
- [22]. Zhang Y., "Adaptive Image Segmentation Based on Fast Thresholding and Image Merging", *Artificial reality and Telexistence-Workshops*, pp. 308-311. 1994.
- [23]. N. R. Pal, "A Review on Image Segmentation Techniques", *Pattern Recognition*. Vol. 26, No. 9, pp. 1277-1294, 1993.
- [24]. S.S. Varshney, N. Rajpal, R. Purwar, "Comparative Study of Image Segmentation Techniques and Object Matching using Segmentation", Proceeding of *International Conference on Methods and Models in Computer Science* , pp. 1-6, 2009.
- [25]. L. Aurdal. "Image Segmentation beyond Thresholding", Norsk Regnesentral: Norwegian Computing Center, 2006.
- [26]. M. Pascal, "Influence of the noise model on level set active contour segmentation", *IEEE Transactions on Pattern Analysis and Machine Intelligence*. Vol. 26, No. 6, pp. 799-803, 2004.